HHS Public Access

Author manuscript

Int Conf Manip Autom Robot Small Scales. Author manuscript; available in PMC 2024 July 01.

Published in final edited form as:

Int Conf Manip Autom Robot Small Scales. 2023 October ; 2023: . doi:10.1109/marss58567.2023.10294125.

Programmable Modular Acoustic Microrobots

Subrahmanyam Cherukumilli[1], **Fatma Ceren Kirmizitas**[*,1,2], **Max Sokolich**[1], **Alejandra Valencia**[*,1], **M. Çağatay Karakan**[3], **Alice E. White**[4] **[Fellow, IEEE]**, **Andreas A. Malikopoulos**[1] **[Senior Member, IEEE]**, **Sambeeta Das**[1] **[Member IEEE]**

[1]Department of Mechanical Engineering, University of Delaware, Newark, DE 19716 USA

[2]Department of Animal and Food Sciences, University of Delaware, Newark, DE 19716 USA

[3]Department of Biomedical Engineering, Boston University, Boston, MA 02215 USA

[4]Department of Mechanical Engineering, and the departments of Biomedical Engineering and Materials Science and Engineering, Boston University, Boston, MA 02215 USA

Abstract

Microrobots have emerged as promising tools for biomedical and in vivo applications, leveraging their untethered actuation capabilities and miniature size. Despite extensive research on diversifying multi-actuation modes for single types of robots, these tiny machines tend to have limited versatility while navigating different environments or performing specific tasks. To overcome such limitations, self-assembly microstructures with on-demand reconfiguration capabilities have gained recent attention as the future of biocompatible microrobotics, as they can address drug delivery, microsurgery, and organoid development processes. Reversible modular reconfiguration structures require specific arrangements of particles that can assume several shapes when external fields are applied. We show how magnetic interaction can be used to assemble cylindrical microrobots into modular microstructures with different shapes. The motion actuation of the formed microstructure happens due to an external acoustic field, which generates responsive forces in the air bubbles trapped in the inner cavity of the robots. An external magnetic field can also steer these structures. We illustrate these capabilities by assembling the robots into different shapes that can swim and be steered, showing the potential to perform biomedical applications. Furthermore, we confirm the biocompatibility of the cylindrical microrobot used as the building blocks of our microstructure. Exposing Chinese Hamster Ovary cells to our microrobots for 24 hours demonstrates cell viability when in contact with the microrobot.

Index Terms —

Modular microrobots; Programmable microstructure; Magnetic interaction; Acoustic actuation

scchs@udel.edu .

*Equal contribution

I. Introduction

In recent years, the field of micro-robotics has gathered significant attention from researchers due to its promising applications in healthcare and biomedical research. Micro/nano robots are particularly appealing because of their small size and the ability to manipulate them using non-invasive methods [1]–[3]. These tiny robots have shown great potential in various biomedical applications, including drug delivery, tissue growth, tumor treatment, and cell manipulation [4]–[11]. Additionally, advancements in fabrication techniques have enabled printing, joint, and placement of objects at miniature scales [12]–[14]. However, classic microrobots operating in solo-actuation or swarms of robots without interaction [15], lack versatility when navigating non-homogeneous environments or performing multiple tasks for in vivo applications [16]. To overcome these limitations and achieve versatility, efficiency, and the ability to mimic microorganisms' functionalities, microscale self-assembled structures have emerged as a promising concept [17]. By assembling colloidal particles such as microrobots with well-defined shapes, sizes, structures, and actuation modes, modular microrobotics can serve as building blocks for microstructures generation [18]–[21]. The challenges of this new concept are many, on top of the existing ones in microrobotics as non-invasive communication and manipulation techniques; actuating and controlling the response from modular microstructures are open research challenges [20], [22]. While the field of microrobotic control has developed various non-invasive actuation methods, such as light, chemical, magnetic, and acoustic [23]–[27], the most relevant methods for modular applications are magnetic and acoustic actuation. These methods have good performance actuating together [28], they are biocompatible, hence useful for in-vivo scenarios, and can satisfactorily actuate robots with different shapes [29]–[32].

Microrobots have demonstrated remarkable capabilities in biomedical applications at the cellular level, surpassing the abilities of traditional methods. However, reconfigurable modular microstructures have the potential to outperform microrobots in applications such as targeted drug delivery, where the size and shape of a microswimmer structure can significantly impact the speed and displacement when swimming in fluids with flow [16]. Modular microstructures structures also have the potential to act as tweezers, graspers, and object transport capsules [33], characteristics with significant value in several applications such as microsurgery, tissue engineering, cell manipulation, and organoid development.

In this paper, we present a modular microrobot design that utilizes both acoustic and magnetic actuation. Our microrobots have a metallic coating that reacts under the magnetic field, which brings them together according to their polarity, placing them as the building blocks of a microstructure. An external acoustic field actuates this new self-assembled microstructure and can be magnetically steered. The acoustic field interacts with an air bubble trapped in each robot's inner cavity, and the magnetic field can steer the whole structure to change its direction.

The remainder of the paper proceeds as follows. In Section II we present materials and methods for developing this study. In Section III, we present the achieved results and

the respective discussion. In Section IV, we draw concluding remarks and present future research directions. Finally, in Section V we present acknowledgments.

II. Materials and Methods

A. Design and Fabrication of the microrobots

The design of our microrobots was initially inspired by the work presented in [28], and we further developed it as illustrated in Fig. 1. Our microrobot features a cylindrical shape with a strategically designed cavity, giving it acoustic properties. When the microrobot is immersed in a fluid, typically a DI water solution, the cavity acts as a reservoir, trapping and retaining an air bubble. The dome-like shape of the inner cavity allows the microrobot to hold the bubble without the risk of bursting securely. The microrobot's dimensions were 40 μm long and 20 μm in diameter. The dimensions were determined to allow the microrobots for smooth interaction with cells when performing drug delivery or cell transportation tasks.

The microrobots were fabricated using the two-photon direct laser writing technique (Nanoscribe Photonic Professional GT) equipped with a 63× objective (NA=1.4), and IP-Dip was used as the photoresist. Microrobots were printed on a diced silicon chip as a 20×20 array with a layer resolution of ≈ 0.4 μm (Fig. 1b). Subsequently, the residual resist was removed from the chip and the microrobots by placing the chips vertically into a propylene glycol monomethyl ether acetate bath for >1 hour, followed by >10 minutes in an isopropanol bath. The remaining solvent was cleaned from the microrobots by dipping the chip into a NOVEC 7100 (3M) bath for a minute and slowly removing it (Fig. 1c).

We coated the microrobots with 100 nm nickel using the Dual vapor E-BEAM deposition technique to impart magnetic responsiveness to the microrobots. Since the nickel vapor is deposited perpendicular to the silicon wafer, it resulted in the half coating of the microrobots. This nickel layer allows us to use an external magnetic field control system. In summary, our microrobots' design and fabrication process involved carefully considering the cylindrical shape, the acoustic cavity for air bubble trapping, and incorporating a half-coated nickel layer for magnetic control.

B. Movement of the Microrobot

The movement of our microrobots is accomplished through the combined effects of external magnetic and acoustic fields.

1) Magnetic Actuation Principle: The magnetic actuation of our microrobot is achieved by applying an external magnetic field. Three pairs of coils are strategically positioned along each Cartesian axis to generate this magnetic field, forming a 3D Helmholtz Coil system. This coil system allows us to establish a joint magnetic field by controlling the three components: $\boldsymbol{B_x}$, $\boldsymbol{B_y}$, and $\boldsymbol{B_z}$. We can direct the magnetic field by applying a controlled time-varying sinusoidal current to each pair of coils, as proposed in [34]. The components can be derived using

$$\boldsymbol{B_x} = -\boldsymbol{B}[\cos(\gamma)\cos(\alpha)\cos(\omega t) + \sin(\alpha)\sin(\omega t)]$$

(1)

$$\boldsymbol{B}_y = -\boldsymbol{B}[\cos(\gamma)\sin(\alpha)\cos(\omega t) - (\cos(\alpha)\sin(\omega t))]$$

(2)

$$\boldsymbol{B}_z = \boldsymbol{B}\sin(\gamma)\cos(\omega t),$$

(3)

where γ is the azimuthal angle from the z axis, α is the polar angle from the x axis, B is the magnetic field magnitude, and ω is the frequency of the field. The default γ is 90°, and changing α allows us to steer the microrobots when actuating under magnetic control. For this magnetic application, the component of the microrobot's magnetic moment parallel to its length synchronizes with the magnetic field [35], and the component perpendicular to its length instigates a rotational movement in the microrobot. This movement is achieved by increasing the frequency ω. The magnetic moment of any object under a magnetic field action is related to the torque, which the expression can represent

$$\boldsymbol{\tau} = \boldsymbol{\mu} \times \boldsymbol{B},$$

(4)

where μ is the Magnetic moment, and B is the Magnetic Field.

As shown in Fig. 2, the torque expressed in (4) induces a rotational motion when the magnetic field is enabled, allowing the microrobot to move within the workspace. We can control the microrobot's motion by precisely controlling the magnetic field parameters, such as direction, magnitude, and frequency. This magnetic control mechanism represents a reliable and efficient means of achieving controlled and directed movement for our microrobots.

2) Acoustic Actuation Principle: Our microrobot's actuation requires a piezoelectric transducer and a signal generator that generate waves at several frequencies. When an acoustic field is enabled, the air bubbles inside each microrobot experience pulsations that generate three distinct forces. Two of these forces significantly impact the robot's motion: the streaming propulsion force and the secondary Bjerknes force [28], [36], [37]. The streaming propulsion force points toward the closed end of the microrobot's cavity and can propel it forward. On the other hand, the secondary Bjerknes force attracts the microrobot toward nearby rigid surfaces [38]. Thus, when the acoustic field is enabled at the resonant frequency of the microrobots, the secondary Bjerknes force gives rise to the formation of a reflected bubble that oscillates in synchronization with the real bubble, as a consequence of acoustic wave scattering [28]. This attracts the robot to a nearby rigid surface, as the force brings the two bubbles together.

Consequently, the actuation mechanism relies on the principle of resonance. As stated before, an air bubble is trapped inside the microrobot's cavity, oscillating at a specific frequency in response to the acoustic waves emitted by the transducers. When the frequency of the field matches the resonant frequency of the bubble, the bubble will keep oscillating constantly, experiencing the two forces priorly explained. Moreover, capillary forces exert pressure on the walls of the microrobot as the bubble oscillates, generating a thrust that enhances the movement of the microrobot. Therefore, by adjusting the frequency of the transducer, we gain control over the microrobot's movement as the resonance and oscillation of the bubble can be modulated. These also affect the magnitude of the exerted capillary forces and the generated thrust. This process gives us control over the acoustic actuation, representing a versatile means for manipulating the microrobot.

As pictured in Fig. 3, the propulsion of the microrobot only happens when an acoustic field is enabled, while the magnetic field allows rolling motion and steering maneuvers.

By carefully adjusting the parameters of the acoustic frequency and the magnetic field, we can manipulate the motion and behavior of the microrobots, harnessing their acoustic and magnetic characteristics for specific applications. This combination of external magnetic control and acoustic actuation offers precise manipulation and transportation of microrobots.

C. Control System

An open-loop control system controls the actuation of the microrobots. The computational capabilities are handled by the Raspberry Pi module and a custom-based controller, as presented in [34] and used in [10], [14], [24]. The coil system described in section II-B is powered by H-bridge PWM drivers connected to the GPIOs. These H-Bridges convert the user-defined currents generated from the GPIO pins and scale them accordingly to each coil. The acoustic actuation is controlled by a DDS signal generator module and a piezoelectric transducer that translates the generated waves into an acoustic field.

D. Cell Culture Studies

Chinese Hamster Ovary (CHO) cells were used as a representative cell line to assess the cytocompatibility of the acoustic modular microrobots. Cells were maintained to grow in Dulbecco's Modified Essential Medium/Nutrient Mixture F-12 (DMEM/F-12, Gibco, BenchStable, USA) supplemented with 10% and 1% penicillin-streptımycin in a humidified cell culture incubator at 37 °C and with %5 CO_2. Cell viability was assessed via trypan blue staining assay after the third passage and before they reached %90 cell density. Cells were seeded into a 6-well plate (Costar, Corning, USA) in a density of 1×10^5 cells/ml per well. Since it is known that the adherent cells tend to detach the growth surface when they are dead, the media was collected after incubation. The culture media was centrifuged and resuspended in Phosphate Buffer Saline (PBS) (Gibco, BenchStable, USA). A 10 μl of cell suspension was mixed with an equal volume of 0.4% trypan blue. Cells were counted using a cell counter (Nexcelom Cellometer Vision Trio Cell Profiler, USA), and cell morphology after staining was observed under an optical microscope (ZOE Fluorescent Cell Imager, USA).

E. Experimental Setup

To perform the experiments, the microrobots were placed in a 3-axis Helmholtz coil system, providing a uniform magnetic field at the center. This involves rotating homogeneous fields, which are generated by controlling the components described in (1), (2), and (3). For details on how the system was developed, see [34]. For our experiments, the samples were placed on a glass slide to which an acoustic transducer was fixed. The microrobots were deposited at the center of the acoustic transducer, mounted in the structure seen in Fig. 4 using a pipette.

III. Results and Discussion

A. Designed Microrobot Motion

The initial experiments were done to understand the movement of the microrobot under the influence of magnetic and acoustic fields. To understand the actuation of the microrobot under the magnetic field, the microrobot is placed on the glass slide along with distilled water. The rolling and spinning properties of the microrobot are studied by applying sinusoidal varying magnetic fields to the Helmholtz coil system. Later, the acoustic fields are applied using a DDS Signal Generator through the transducer fixed to the glass slide. We empirically found the resonant frequency of the bubble inside the dome-like structure by performing a frequency sweep using the signal generator, which helps navigate the microrobot.

B. Demonstration of Modular Microrobots Motion and Interaction

After understanding the feasibility of the microrobot design to actuate by both magnetic and acoustic fields, a group of microrobots is carefully placed on the glass slide in the distilled water, and the Helmholtz coil system is powered, which generates a magnetic field. When intermittent magnetic fields are applied to the non-uniformly dispersed microrobots, the microrobots experience dipole attractions between each other due to the 100 nm nickel coating. The dipole-dipole interactions arising from the half-coated nickel layer of the cylindrical microrobots drive these units to engage with each other, thereby initiating the formation of modular assemblies. The distance between the cylinders, the magnetic field strength, and the number of microrobots units influence the modular units' formation. After the shape is formed, the acoustic field manages the motion of the microstructure, as shown in Fig. 5, which provides an overview of the formation of modular microstructures.

To show the experimental validation of the schematic exposed in Fig. 5, sinusoidal varying magnetic currents are applied to the Helmholtz system, making the microrobots rotate and spin. This interaction resulted in the formation of shapes such as "L", and "T"(cross). The process in the robots is shown in Fig. 6, where Fig. 6a represents the initial state of the microrobots under no actuation, Fig. 6b shows when the magnetic field is enabled, and Fig. 6c–f shows the formed microstructures.

The modular units attain stability once the dipole attractions and the viscous and drag forces acting on the microrobots reach equilibrium. The shapes remain stable due to the external magnetic field and the dipole attractions caused by the ferromagnetic nature of the nickel.

The modular units can be programmed by applying varying magnetic fields, although it also depends on the number of microrobots near each other. The modular units formed can be steered by applying rotating and spinning magnetic fields. The actuation of the modular units is achieved by enabling the acoustic field at the resonating frequency of the bubbles inside the dome-like structure of the microrobot. As shown in Fig. 7, the microstructure will remain together due to the magnetic field, while swimming under the acoustic actuation.

These experimental results hold promise for using microrobots in various applications, such as cell manipulation, cell delivery, and tissue generation, taking advantage of the modular units formed by the microrobots.

C. Cell Viability

Cytocompatibility is one of the major concerns for all potential microrobots for biomedical applications. It is necessary to be assured that the microrobots are non-toxic and well tolerated by the living cells. In this study, we used a trypan blue staining assay to determine the cytocompatibility of the acoustic modular microrobots. Microrobots were with the cells for 24 hours under standard culture conditions. Fig. 8 shows the images of the cell viability results of the acoustic microrobots. The morphology and proliferation of microrobot-treated cells were intact after 24 hours of incubation compared to the control cells. Also, cell viability for microrobot-treated CHO cells was assessed and found as 91%, as shown in Fig. 8, and when compared with the control cells live/dead cell ratio was negligible. The results clearly revealed that the presented acoustic modular microrobot can be a potential candidate for future biomedical applications.

IV. Conclusion

In this work, we successfully demonstrated the actuation capabilities of a new microrobot design that combines magnetic and acoustic modes. The microrobots were specifically designed to be biocompatible and easily manipulated. Besides the acoustic actuation mode inherent to the capsule-like design of the robot, magnetic actuation was desired. By incorporating a nickel coating on the microrobots, they exhibited desired magnetic response while maintaining their acoustic properties and overall functionality. The hybrid design of these microrobots offers versatility in manipulation and control strategies, making them highly suitable for a wide range of biomedical and in vivo applications. Experimental results showcased the performance of the microrobots when shaped as microstructures, enabling effective cell manipulation under open-loop control. Further research is necessary to explore the implementation of these microstructures in more complex systems. Future investigations should focus on enhancing the functionality, precision, and adaptability of the microrobots to meet the evolving demands of biomedical applications. By continuing to advance the understanding and capabilities of these modular microrobots, significant progress can be made in biomedical engineering and in vivo applications.

Acknowledgements

The authors gratefully acknowledge Dr. Zameer Hussain Shah for his valuable help in this work. They also thank QNF, the University of Pennsylvania, and Boston University for their technical support in the realization of the study. This work was supported by the National Science Foundation under grant GCR 2219101 and the National

Health Institute under grant 1R35GM147451. This project was also supported with a grant from the National Institute of General Medical Sciences – NIGMS (5P20GM109021-07) from the National Institutes of Health and the State of Delaware. MÇK and AEW were supported by the NSF Engineering Research Center on Cellular Metamaterials (CELL-MET; EED-1647837).

References

[1]. Shah ZH, Wu B, and Das S, "Multistimuli-responsive microrobots: A comprehensive review," Frontiers in Robotics and AI, vol. 9, p. 1027415, 2022.

[2]. Nelson BJ, Kaliakatsos IK, and Abbott JJ, "Microrobots for minimally invasive medicine," Annual review of biomedical engineering, vol. 12, pp. 55–85, 2010.

[3]. Sitti M, "Voyage of the microrobots," Nature, vol. 458, no. 7242, pp. 1121–1122, 2009. [PubMed: 19407789]

[4]. Aziz A, Pane S, Iacovacci V, Koukourakis N, Czarske J, Menciassi A, Medina-Sánchez M, and Schmidt OG, "Medical imaging of microrobots: Toward in vivo applications," ACS nano, vol. 14, no. 9, pp. 10 865–10 893, 2020.

[5]. Jeong J, Jang D, Kim D, Lee D, and Chung SK, "Acoustic bubble-based drug manipulation: Carrying, releasing and penetrating for targeted drug delivery using an electromagnetically actuated microrobot," Sensors and Actuators A: Physical, vol. 306, p. 111973, 2020.

[6]. Park J, Kim J.-y., Pané S, Nelson BJ, and Choi H, "Acoustically mediated controlled drug release and targeted therapy with degradable 3d porous magnetic microrobots," Advanced healthcare materials, vol. 10, no. 2, p. 2001096, 2021.

[7]. Sitti M, Ceylan H, Hu W, Giltinan J, Turan M, Yim S, and Diller E, "Biomedical applications of untethered mobile milli/microrobots," Proceedings of the IEEE, vol. 103, no. 2, pp. 205–224, 2015. [PubMed: 27746484]

[8]. Dogangil G, Davies B, and Rodriguez y Baena F, "A review of medical robotics for minimally invasive soft tissue surgery," Proceedings of the Institution of Mechanical Engineers, Part H: Journal of Engineering in Medicine, vol. 224, no. 5, pp. 653–679, 2010. [PubMed: 20718269]

[9]. Wu Z, Troll J, Jeong H-H, Wei Q, Stang M, Ziemssen F, Wang Z, Dong M, Schnichels S, Qiu T et al. , "A swarm of slippery micropropellers penetrates the vitreous body of the eye," Science advances, vol. 4, no. 11, p. eaat4388, 2018. [PubMed: 30406201]

[10]. Mallick S, Abouomar R, Rivas D, Sokolich M, Kirmizitas FC, Dutta A, and Das S, "Doxorubicin-loaded microrobots for targeted drug delivery and anticancer therapy." Advanced Healthcare Materials, pp. e2 300 939–e2 300 939, 2023.

[11]. Rahman MM, Garudadri T, and Das S, "Role of surface tension in microrobot penetration in membranes," in 2022 International Conference on Manipulation, Automation and Robotics at Small Scales (MARSS). IEEE, 2022, pp. 1–6.

[12]. Li J and Pumera M, "3d printing of functional microrobots," Chemical Society Reviews, vol. 50, no. 4, pp. 2794–2838, 2021. [PubMed: 33470252]

[13]. Cabanach P, Pena-Francesch A, Sheehan D, Bozuyuk U, Yasa O, Borros S, and Sitti M, "Zwitterionic 3d-printed non-immunogenic stealth microrobots," Advanced Materials, vol. 32, no. 42, p. 2003013, 2020.

[14]. Shah ZH, Sockolich M, Rivas D, and Das S, "Fabrication and open-loop control of three-lobed nonspherical janus microrobots," MRS Advances, pp. 1–5, 2023. [PubMed: 37362909]

[15]. Beaver LE, Wu B, Das S, and Malikopoulos AA, "A first-order approach to model simultaneous control of multiple microrobots," in 2022 International Conference on Manipulation, Automation and Robotics at Small Scales (MARSS). IEEE, 2022, pp. 1–7.

[16]. Cheang UK, Meshkati F, Kim H, Lee K, Fu HC, and Kim MJ, "Versatile microrobotics using simple modular subunits," Scientific reports, vol. 6, no. 1, pp. 1–10, 2016. [PubMed: 28442746]

[17]. Cademartiri L and Bishop KJ, "Programmable self-assembly," Nature materials, vol. 14, no. 1, pp. 2–9, 2015. [PubMed: 25515989]

[18]. Grzelczak M, Vermant J, Furst EM, and Liz-Marzán LM, "Directed self-assembly of nanoparticles," ACS nano, vol. 4, no. 7, pp. 3591–3605, 2010. [PubMed: 20568710]

[19]. Kaiser A, Snezhko A, and Aranson IS, “Flocking ferromagnetic colloids,” Science advances, vol. 3, no. 2, p. e1601469, 2017. [PubMed: 28246633]

[20]. Han K, Shields IV CW, Diwakar NM, Bharti B, López GP, and Velev OD, “Sequence-encoded colloidal origami and microbot assemblies from patchy magnetic cubes,” Science advances, vol. 3, no. 8, p. e1701108, 2017. [PubMed: 28798960]

[21]. Rivas DP, Sokolich M, and Das s., “Spatial patterning of micromotor aggregation and flux,” ChemNanoMat, p. e202300225. [PubMed: 38292294]

[22]. Li D, Chen Q, Chun J, Fichthorn K, De Yoreo J, and Zheng H, “Nanoparticle assembly and oriented attachment: correlating controlling factors to the resulting structures,” Chemical Reviews, vol. 123, no. 6, pp. 3127–3159, 2023. [PubMed: 36802554]

[23]. Das S, Hunter EE, DeLateur NA, Steager EB, Weiss R, and Kumar V, “Cellular expression through morphogen delivery by light activated magnetic microrobots,” Journal of Micro-Bio Robotics, vol. 15, pp. 79–90, 2019.

[24]. Sokolich M, Rivas D, Shah ZH, and Das S, “Automated control of catalytic janus micromotors,” MRS Advances, pp. 1–5, 2023. [PubMed: 37362909]

[25]. Jiang J, Yang Z, Ferreira A, and Zhang L, “Control and autonomy of microrobots: Recent progress and perspective,” Advanced Intelligent Systems, vol. 4, no. 5, p. 2100279, 2022.

[26]. Das S, Hunter EE, DeLateur NA, Steager EB, Weiss R, and Kumar V, “Controlled delivery of signaling molecules using magnetic microrobots,” in 2018 international conference on manipulation, automation and robotics at small scales (MARSS). IEEE, 2018, pp. 1–5.

[27]. Das S, Steager EB, Stebe KJ, and Kumar V, “Simultaneous control of spherical microrobots using catalytic and magnetic actuation,” in 2017 International Conference on Manipulation, Automation and Robotics at Small Scales (MARSS). IEEE, 2017, pp. 1–6.

[28]. Ren L, Nama N, McNeill JM, Soto F, Yan Z, Liu W, Wang W, Wang J, and Mallouk TE, “3d steerable, acoustically powered microswimmers for single-particle manipulation,” Science advances, vol. 5, no. 10, p. eaax3084, 2019. [PubMed: 31692692]

[29]. Xu T, Yu J, Yan X, Choi H, and Zhang L, “Magnetic actuation based motion control for microrobots: An overview,” Micromachines, vol. 6, no. 9, pp. 1346–1364, 2015.

[30]. Fischer P and Ghosh A, “Magnetically actuated propulsion at low reynolds numbers: towards nanoscale control,” Nanoscale, vol. 3, no. 2, pp. 557–563, 2011. [PubMed: 21152575]

[31]. Aghakhani A, Yasa O, Wrede P, and Sitti M, “Acoustically powered surface-slipping mobile microrobots,” Proceedings of the National Academy of Sciences, vol. 117, no. 7, pp. 3469–3477, 2020.

[32]. Rivas D, Mallick S, Sokolich M, and Das S, “Cellular manipulation using rolling microrobots,” in 2022 International Conference on Manipulation, Automation and Robotics at Small Scales (MARSS). IEEE, 2022, pp. 1–6.

[33]. Zheng Z, Wang H, Demir SO, Huang Q, Fukuda T, and Sitti M, “Programmable aniso-electrodeposited modular hydrogel microrobots,” Science Advances, vol. 8, no. 50, p. eade6135, 2022. [PubMed: 36516247]

[34]. Sokolich M, Rivas D, Yang Y, Duey M, and Das S, “Modmag: A modular magnetic micro-robotic manipulation device,” MethodsX, vol. 10, p. 102171, 2023.

[35]. Liao H, Liu X, Liu D, Ning Y, Huang Q, and Arai T, “Magnetically driven rolling motion for magnetic cylindrical microrobots,” in 2021 IEEE International Conference on Mechatronics and Automation (ICMA). IEEE, 2021, pp. 976–980.

[36]. Ahmed D, Baasch T, Jang B, Pane S, Dual J, and Nelson BJ, “Artificial swimmers propelled by acoustically activated flagella,” Nano letters, vol. 16, no. 8, pp. 4968–4974, 2016. [PubMed: 27459382]

[37]. Bertin N, Spelman TA, Stephan O, Gredy L, Bouriau M, Lauga E, and Marmottant P, “Propulsion of bubble-based acoustic microswimmers,” Physical Review Applied, vol. 4, no. 6, p. 064012, 2015.

[38]. Moo JGS, Mayorga-Martinez CC, Wang H, Teo WZ, Tan BH, Luong TD, Gonzalez-Avila SR, Ohl C-D, and Pumera M, “Bjerknes forces in motion: Long-range translational motion and chiral directionality switching in bubble-propelled micromotors via an ultrasonic pathway,” Advanced Functional Materials, vol. 28, no. 25, p. 1702618, 2018.

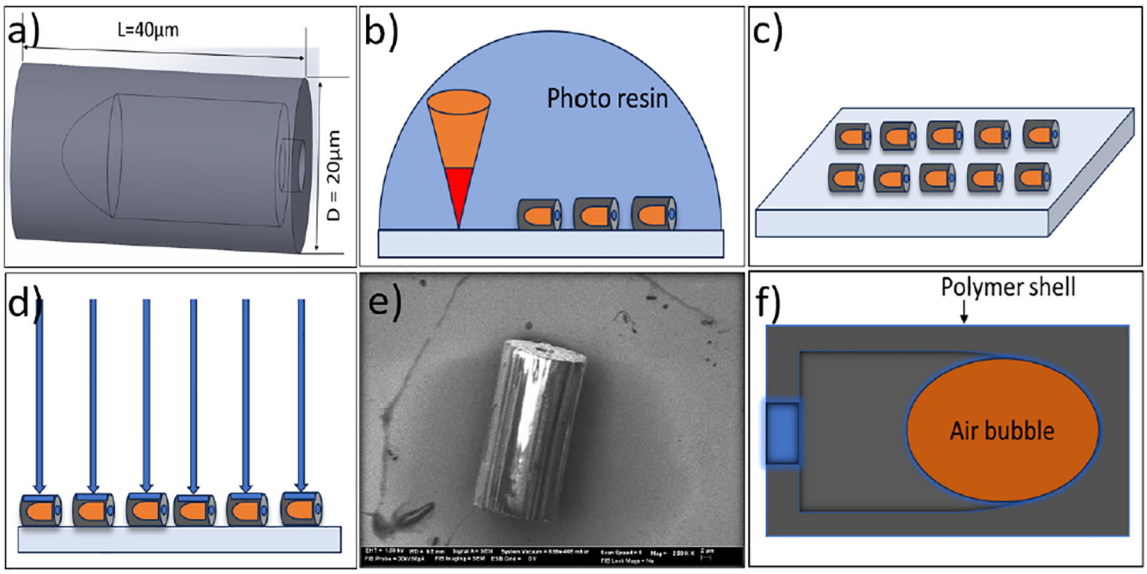

Fig. 1:

Design and Fabrication process. a) Overview of the microrobot design b) 3D printing microrobots on a silicon chip using a two-photon direct laser writing technique. c) Overview of the printed microrobots on the silicon chip after removing the excess resin. d) Illustration of the nickel vapor deposition on the silicon chip e) The scanning electron microscope image of the nickel-layer deposited microrobot f) The sectional view of the microrobot with the air bubble in DI water solution

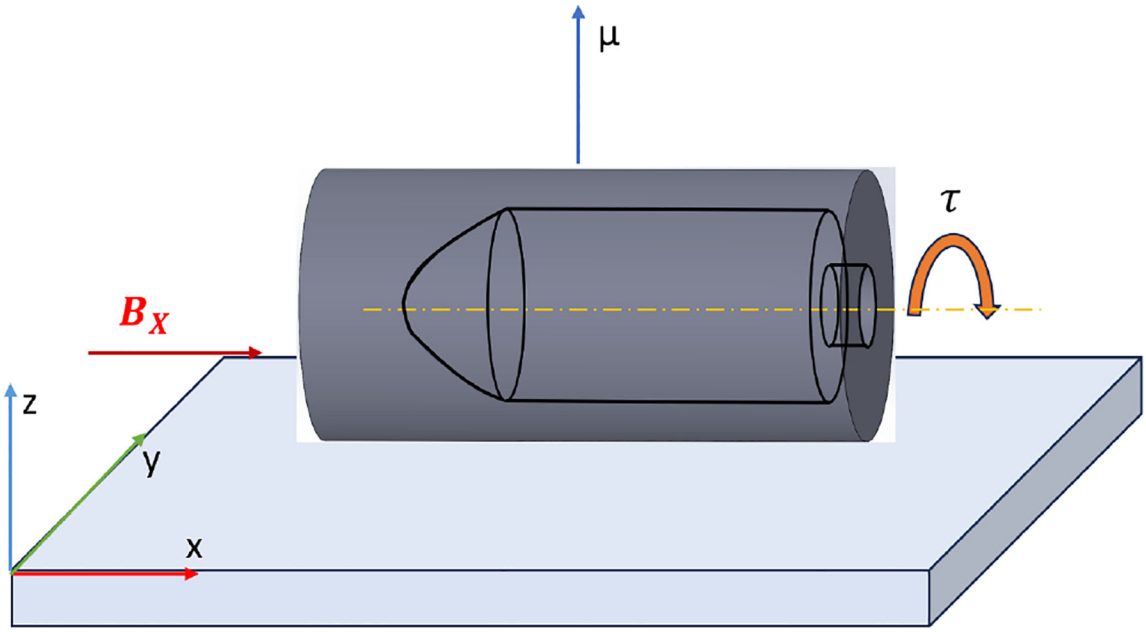

Fig. 2:
The rolling motion of the microrobot

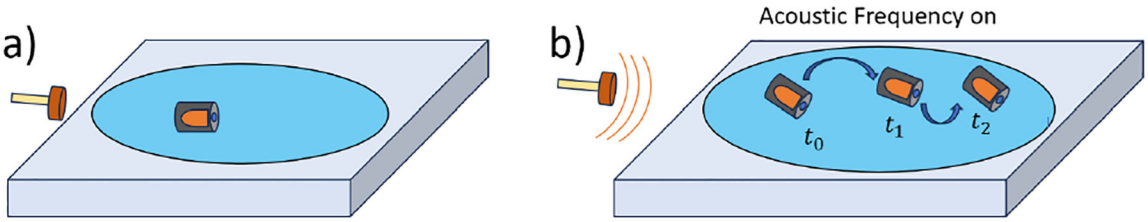

Fig. 3:

Acoustic Schematic. a) The initial position of the microrobot. b) Movement of the microrobot over time by applying acoustic frequency

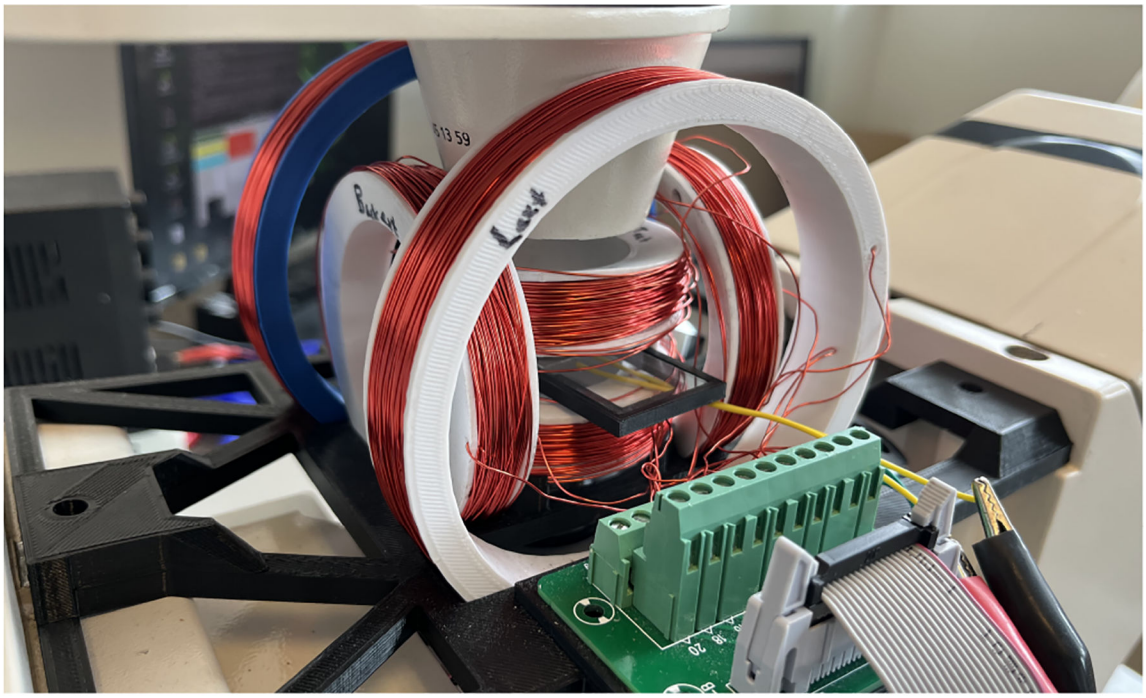

Fig. 4:
Experimental Setup.

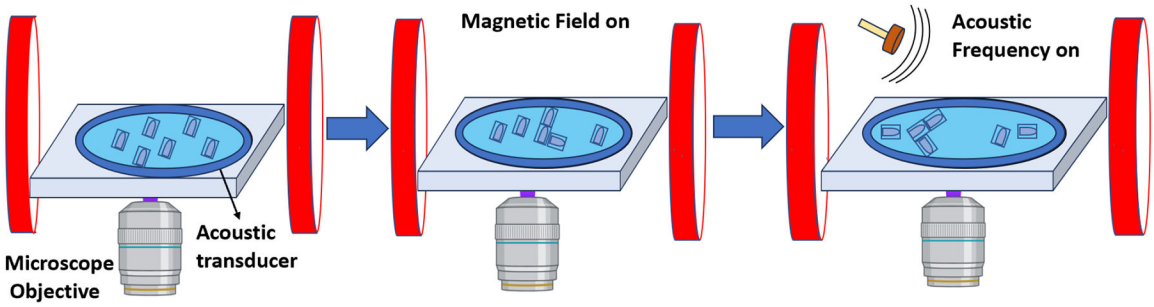

Fig. 5:

Schematic of the modular units formation by the magnetic field and actuation of the modular units using acoustic frequency

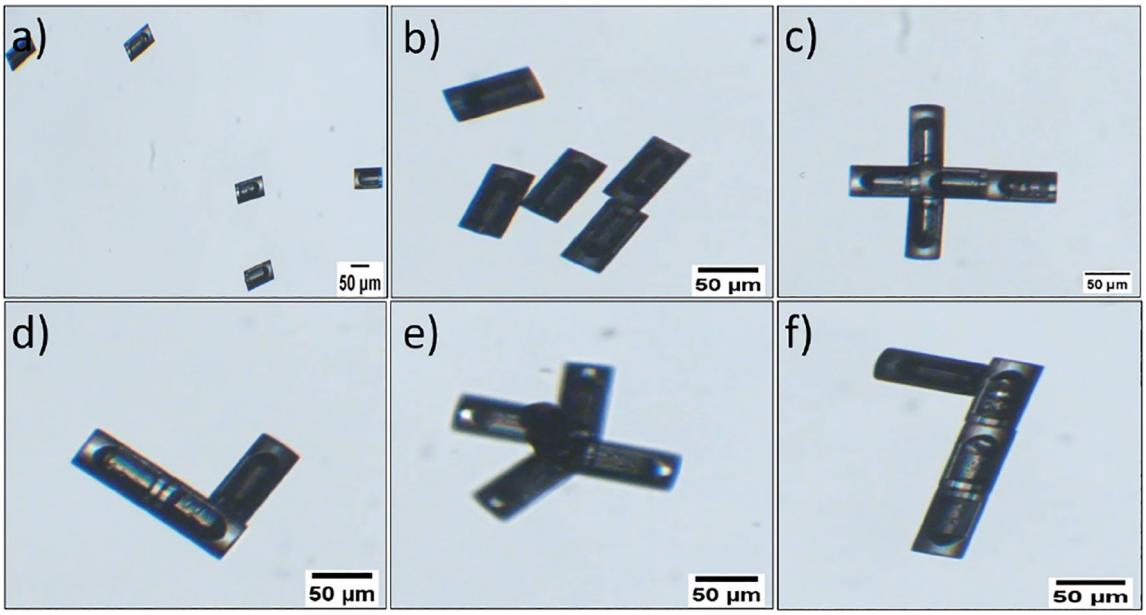

Fig. 6:

Formation of the modular units. a) Initial state of microrobots after placing on glass slide b) Microrobots under the magnetic field. c,d,e,f)Various shapes were programmed during the experiments.

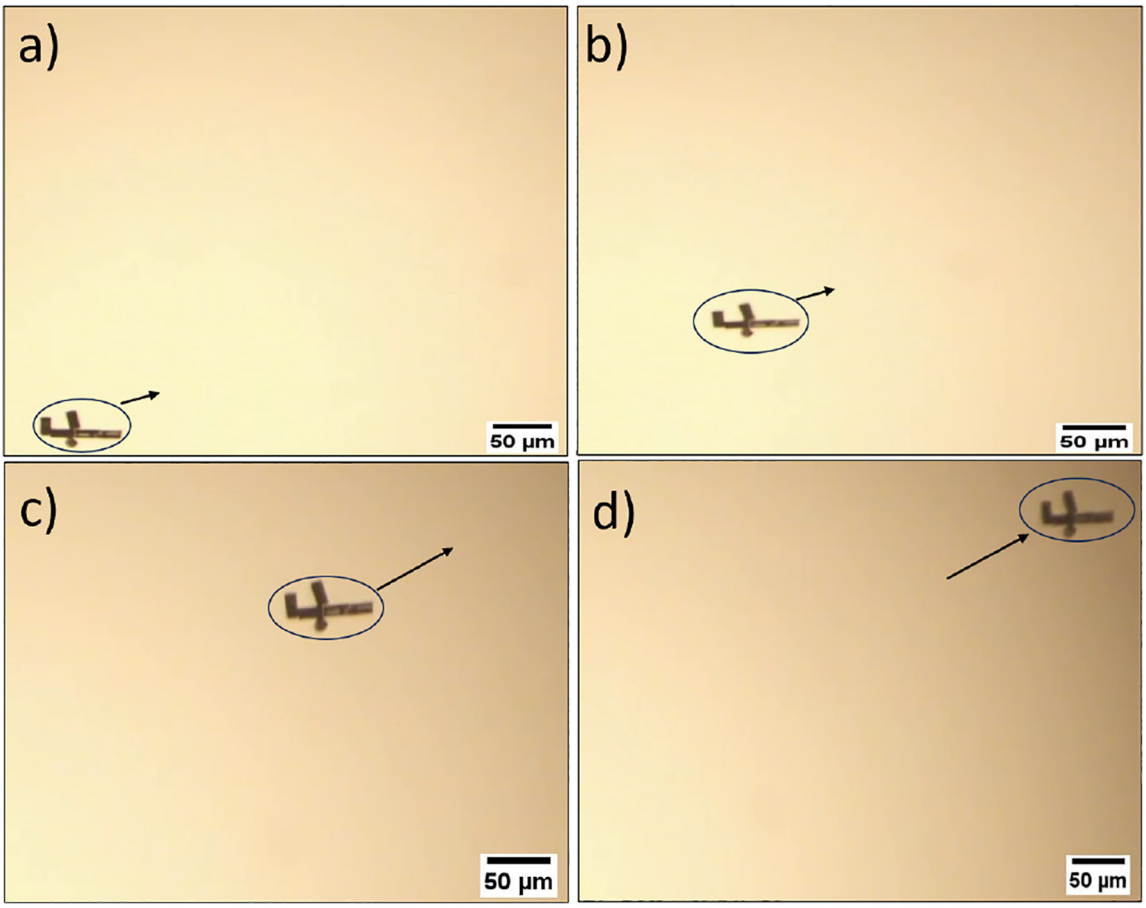

Fig. 7:
Frames showing the Acoustic actuation of the modular microrobot

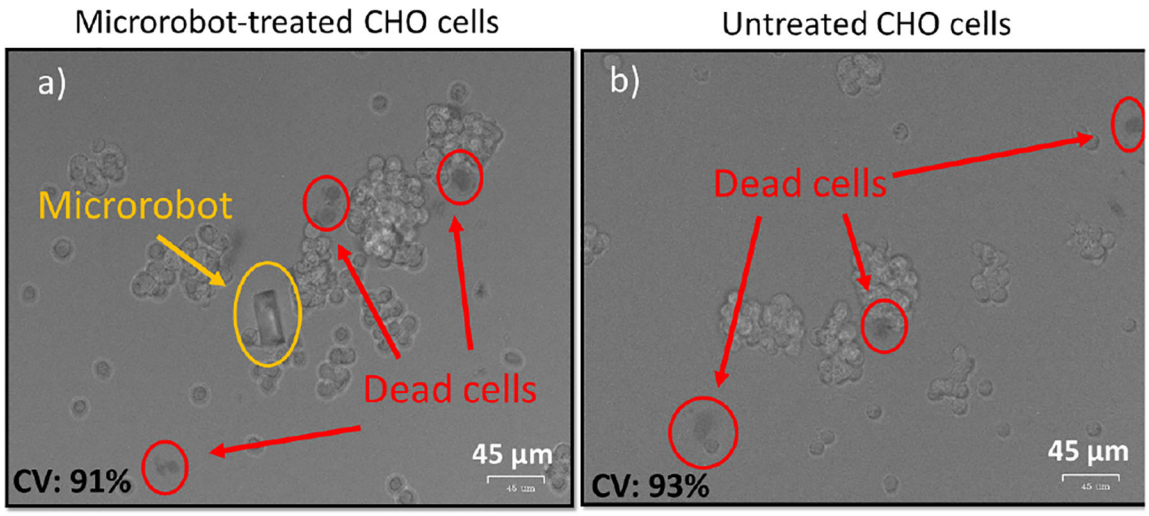

Fig. 8:

Images of microrobot-treated (a) and untreated (b) CHO cells. Cell viability was 91%, and the dead cells are stained and shown in red circles. CV represents cell viability.